

# Regional dynamical downscaling with CCLM over East Asia

Dinan Wang · Christoph Menz · Thorsten Simon ·  
Clemens Simmer · Christian Ohlwein

Received: 24 April 2012 / Accepted: 22 March 2013 / Published online: 23 April 2013  
© Springer-Verlag Wien 2013

**Abstract** Inspired by the framework of the Coordinated Regional Climate Downscaling Experiment (CORDEX), the hindcast (1971–2000) and projection (2021–2050) simulations based on a resolution of  $0.44^\circ$  over the East Asia domain are performed with the regional climate model COSMO-CLM (CCLM). The simulations are driven by ERA-40 reanalysis data and output of the global climate model ECHAM5. This is the first time that the CCLM is adapted and evaluated for the East Asia Monsoon region; the setup is considered a starting point for further improvements in this region by the CCLM community. The evaluation results show that the CCLM is able to reasonably capture the climate features in this region, especially the monsoon dynamics on small scales. However, total precipitation in the northern part of the domain, over the Tibetan Plateau, and over east Indonesia has a pronounced wet bias. The projected climate change under the A1B scenario indicates an overall annual surface temperature increase of 1–2 K, but no significant precipitation changes.

## 1 Introduction

The first successful application of regional climate models (RCM) dates back almost two decades (Giorgi and Bates 1989). Particularly in the last decade, considerable community efforts have been invested into improvement of model physics and dynamics for meso-scale processes and into the investigation of internal model variability and model limitations, while the range of RCM application has steadily increased (Rummukainen 2010). Despite these efforts and the potential of RCMs to reveal climate changes on the scales required for impact studies, the merits of dynamical downscaling (downscaling of global climate simulations with RCMs) are often debated. Concerns can mostly be related to the isolated regional climate downscaling studies over specific interested areas and the lack of ensemble projections of sufficient quality (Giorgi et al. 2009). Intrigued by these debates, World Climate Research Program (WCRP) recently initiated the coordinated regional climate downscaling experiment (CORDEX)<sup>1</sup>, which will provide a comprehensive picture of regional climate change projections based on ensembles of dynamical downscaling experiments.

In our regional climate downscaling studies over East Asia, we largely follow the rules recommended by CORDEX. The study region covers the area of interest of the two research programmes co-funded by the German Research Foundations and the National Natural Science Foundation of China (DFG/NSFC, “Land Use and Water Resources Management under Changing Environmental Conditions”, 2010–2012) and by the German Federal Ministry for Research and Education (BMBF, “Sustainable water and agricultural land use in the Guanting watershed

---

Responsible editor: J.-F. Miao.

---

D. Wang · T. Simon · C. Simmer · C. Ohlwein  
Meteorological Institute, University of Bonn, Auf dem Hügel 20,  
Bonn 53121, Germany

*Present Address:*

D. Wang (✉)  
Institute of Energy Systems and Energy Business, Hochschule  
Ruhr-West - University of Applied Sciences, Tannenstr. 43,  
Bottrop 46240, Germany  
e-mail: dinanbonn@yahoo.de

C. Menz  
Potsdam Institute for Climate Impact Research, Potsdam,  
Germany  
e-mail: menz@pik-postdam.de

<sup>1</sup> [http://wcrp.ipsl.jussieu.fr/SF\\_RCD\\_CORDEX.html](http://wcrp.ipsl.jussieu.fr/SF_RCD_CORDEX.html).

under limited water resources”, 2009–2012). The aim of the DFG/NSFC project hosted by the University of Bonn is the combination of dynamical and statistical downscaling of global climate runs for a better understanding of potential future extreme events in the Haihe and Poyang Lake watersheds in China. The BMBF project, hosted by Potsdam Institute for Climate Impact Research, also employs a similar approach to the Guanting watershed. The downscaling results will be used to force hydrological models employed within the two research programmes. Since the simulation domains of both programmes are located within the East Asia domain defined by CORDEX, we performed a series of regional dynamical downscaling runs over this area. Although inspired by CORDEX, our simulation setups are not identical to the prescriptions by CORDEX (e.g. the domain size and the driving data) due to the priorities of both programmes.

The Asian Summer Monsoon (ASM) is probably the most pronounced regional climate system in the region. The dynamics of ASM influences droughts and floods over Asia and impacts the global circulation (Ji and Vernekar 1997), thus its representation in simulations is of particular concern. Multiple general circulation model (GCM) ensemble simulations are usually employed to quantify the uncertainty range of climate projections (Min et al. 2004; Kitoh and Uchiyama 2006). Due to low spatial resolutions and the required parameterizations, GCMs have difficulties to describe regional precipitation patterns generated by the ASM regions (Kawase et al. 2008; Gao et al. 2006). These problems are likely caused at least in part by heavy rainfall associated with the steep orography (IPCC 2007). The higher spatial resolution of RCMs is expected to remedy some of these shortcomings (Fu et al. 2005; Kumar et al. 2006). For example, Gao et al. (2006) found that even the simulated large scale precipitation patterns are heavily influenced by resolution during the mid- to late-monsoon months, when small scale convective processes dominate precipitation generation. Mesoscale processes in the RCMs are indeed in some cases beneficial for rendering a more clear picture of ASM features (Yhang and Hong 2008).

The regional climate model COSMO-CLM (CCLM: COSMO—the Consortium for Small-scale Modelling, CLM—Climate Limited-area Modelling or climate version of “Lokalmodell”) has been adopted for regional climate change projections in our study by employing the so-called time-slice mode. The CCLM has been already examined for its inter-continent transferability using the standard parameter setup for Europe, in which particularly the tropical ASM region was investigated within a short period (2001–2004) (Rockel and Geyer 2008). Dobler and Ahrens (2008) showed the CCLM capabilities for Indian Summer Monsoon studies. The CCLM has, however, not been configured for East Asia for the investigation of

future climate change, which is the central topic of this paper.

In Sect. 2, the simulation design including study region, model configuration and reference data is described. Section 3 presents the results from five experiments. The analysis focuses on the  $2m$  (screen level) temperature and precipitation. In a subsection, also the capability of the CCLM to model the important East Asia monsoon dynamics on small scales is demonstrated by examples. Section 4 finally provides a short summary and some conclusions from our study.

## 2 Simulation design

### 2.1 Study region

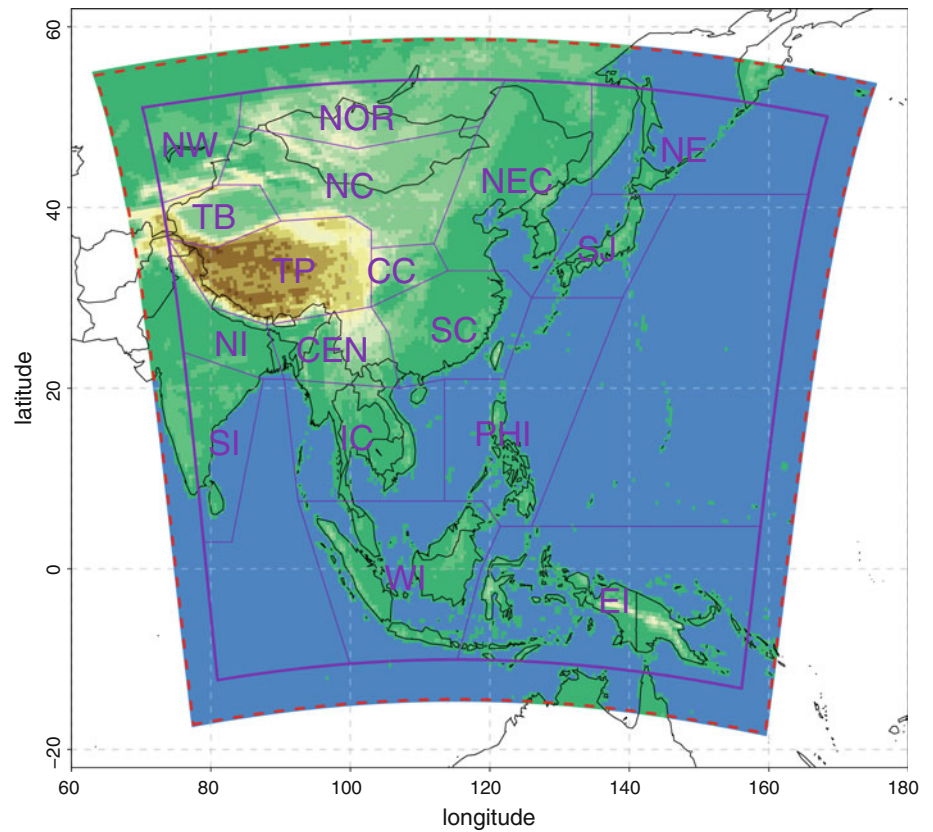
The CORDEX East Asia domain has a spatial extension of roughly  $10,500 \times 8,000 \text{ km}^2$ . Besides China, Mongolia and most parts of India, it covers Indochina and the islands of Indonesia, the Philippines, and Japan. Almost one third of the world’s population inhabits this region. The region is characterized by a large land-sea-contrast stimulating the Monsoon circulation and steep orography modulating the regional circulation and its effects on precipitation patterns. Figure 1 shows the simulation domain of the CCLM (red dotted line). For boundary relaxation and mitigation of gravity, wave reflection the lateral relaxation zone is set to 16 grid boxes ( $\approx 800 \text{ km}$ ) leaving an area of  $9,500 \times 7,000 \text{ km}^2$  (purple line), which we term “CORDEX East Asia (CORDEX-easia)” for evaluation. The continental area is divided into 17 sub-domains, which were chosen according to Köppen–Geiger classification and observed mean temperature and precipitation.

### 2.2 Model configuration

The CCLM is a non-hydrostatic regional climate model for meso- $\beta$  to meso- $\gamma$  scale resolutions (1–50 km). The model is based on the primitive thermo-hydrodynamic equations, which are formulated on a rotated horizontal grid [ARAKAWA-C-lattice type (Arakawa and Lamb 1981)] and a terrain following height coordinate.<sup>2</sup> Table 1 shows the grid definitions for our simulations. Various parameters were tested by two short-term simulations (1959–1964, 1996–1998) excluding the first year, respectively, for spin-up. Both test simulations were driven by ERA-40 reanalysis data to minimise systematic biases introduced from driving models. The period 1996–1998 includes two extreme events, i.e. the drought in the North China Plain in 1997 and the flooding in south China in 1998. The tests,

<sup>2</sup> <http://www.cosmo-model.org>.

**Fig. 1** The study region: the simulation domain of the CCLM is bounded by the red dotted line and the evaluation region is outlined with the solid purple line. For the evaluation purpose, the domain is divided into the following subregions: NW North West, NOR North, NEC North East China, NE North East, TB Tarim Basin, NC North China, CC Central China, SJ South Japan, TP Tibetan Plateau, SC South China, PHI Phillippines, NI North India, SI South India, CEN Central, IC Indochina, WI West Indonesia and EI East Indonesia



based on the standard setup of CCLM for Europe, focused on the selection of the most appropriate integration scheme and the configuration of the lateral and upper boundary relaxation zones. The limited computational resources restricted the test simulations to rather short periods; also potential interdependencies of tested parameters could not be evaluated in detail. Benchmark variables were 2 m temperature and precipitation.

The Leapfrog temporal integration scheme is chosen over the Runge–Kutta scheme, because of both better

computational performance and representation of spatial patterns of temperature and precipitation in particular over China. Different integration time-steps (from 75 to 150 s) were tested; improvements when using smaller time-steps than 150 s were insignificant and did not justify the longer computational time. A modified Robert–Asselin time filter (Williams 2009) (named as “alphaass” in the CCLM) is used in conjunction with the Leapfrog scheme to reduce the impacts of the filter on the physical mode while suppressing the spurious computational mode. Our tests

**Table 1** Grid specifications of the simulations

	Longitude	Latitude
<i>Atmosphere</i>		
<i>Horizontal grid</i>		
Rotated north pole location	−64.78	77.61
Rotated grid extension	−47.96 to 55.44	−33.88 to 53.68
Rotated grid resolution	0.44	0.44
Number of grid points	235	199
<i>Vertical grid</i>		
Number of vertical layers	32	
<i>Soil</i>		
Number of soil layers	10	
Soil layer depth [m]	0.01, 0.035, 0.08, 0.17, 0.35, 0.71, 1.43, 2.87, 5.75, 11.51	

**Table 2** Basic model configuration parameters of the CCLM

Model configuration	
Convection scheme	Tiedtke
Time integration scheme	Leapfrog, time step = 150 s
Robert–Asselin time filter (alphaass)	0.7
Lateral relaxation layer (rlwidth, km)	800
Rayleigh damping layer (rdheight, km)	13
Microphysics scheme	Kessler-type (1969)
Turbulence scheme	Prognostic turbulent kinetic energy (TKE)
Radiation scheme	Ritter and Geleyn (1992)

indicate that the proper adjustment of this filter (alphaass = 0.7) can lead to a significant improvement, especially for the simulated temperatures in Haihe basin.

Steep orography is evident within the CORDEX-easia domain and at the lateral boundaries. Moreover, the simulation domain incorporates a wide range of climatic zones. Thus, it is essential to investigate model sensitivity to specifications of the lateral and upper boundary relaxation zones. The tests on the width of the lateral relaxation layer (named as “rlwidth” in the CCLM) reveal that the high mountains within or close to the lateral relaxation zone result in a significant overestimation of precipitation. The interpolated fields of the driving model seem to produce additional orographic precipitation. We selected an 800 km wide lateral relaxation layer containing the Karakorum. This configuration produces better precipitation patterns within the central area of the model domain and our study regions, despite considerable overestimations of precipitation in a small area near the Karakorum. As the model domain includes tropical and sub-tropical climatic zones as well as the mountainous regions, the Rayleigh sponge damping layer on the top of the model domain needs to be adjusted. The bottom height (named as “rdheight” in the CCLM) of the layer is extended from the standard setup of 11–13 km, which improves particularly monthly precipitation in south China and north east China. The most important CCLM (COSMO\_4.8\_CLM11) parameters found for this study are listed in Table 2.

### 2.3 Reference data

As reference datasets for temperature and precipitation, we use the CRU-TS 3.0 (Climate Research Unit)<sup>3</sup> (Jones and Harris 2008) and APHRODITE-APHRO\_V1003R1 datasets (Asian Precipitation Highly Resolved Observational

Data Integration towards Evaluation of the Water Resources)<sup>4</sup> (Xie et al. 2007). CRU-TS3.0 defined on a  $0.5^\circ \times 0.5^\circ$  grid contains global monthly 2m temperature, while APHRODITE contains daily precipitation over Asia on a  $0.25^\circ$  grid or  $0.5^\circ$  (the latter is used in this paper). APHRO\_V1003R1 is based on the network of daily rain gauge data for Asia, which contains up to 4.5 times more observations than available through the Global Telecommunication System network, and thus should better characterize precipitation characteristics in mountainous areas, such as the Himalayas (Yatagai et al. 2009). For evaluation, the CCLM output is mapped to the CRU-TS3.0 grid ( $0.5^\circ$ ) via a bilinear interpolation.

### 3 Simulation results and analysis

Three hindcast simulations for model evaluation and simulation design are performed, driven by ERA-40 reanalysis data (Uppala et al. 2005) and ECHAM5-20C-(R1, all-R3) (Roeckner et al. 2006a; Roeckner 2005) in a spectral resolution TL159 with 49 atmospheric and three soil layers. ECHAM5 GCM outputs on a T63 grid with 31 atmospheric and 4 soil layers are used for both hindcast and future projections. ECHAM5-20C-all-R3 is forced by anthropogenic (green house gases, sulphate) plus natural forcing (variable solar constant and effects of volcanic aerosols are included), while ECHAM-20C-R1 only includes observed anthropogenic forcing. Hence we can examine the impact of natural forcing on the model response. The A1B emission scenario is used in two simulations with the ECHAM5 global climate model (ECHAM5-A1B-(R1,R3) (Roeckner et al. 2006b, c), to which we apply dynamical downscaling. Both realizations are initialized with different runs of ECHAM5-20C using anthropogenic forcing. Our CCLM simulations for the period from 1971 to 2000 driven either with ERA-40 or ECHAM5-20C are used for validation. For the future projection run, the period from 2021 to 2050 is chosen because of its relevance for near future climate change impact assessments required by the funding research programmes.

Evaluation focuses on the average annual and seasonal 2 m temperature (Fig. 2) and total precipitation fields (Fig. 3). Due to the large spatial variability of annual precipitation over the simulation domain, we compute the relative bias (the difference relative to the respective reference dataset) (Fig. 3). The relative bias is considered significant when the  $p$  value of a  $t$  test (von Storch and Zwiers 1999) is below 0.1. We also show the annual values averaged over the sub-regions defined in Fig. 1.

<sup>3</sup> Data are available online <http://www.cru.uea.ac.uk/cru/data/hrg/>.

<sup>4</sup> Data are available on-line <http://www.chikyu.ac.jp/precip/>.



### 3.1 ERA-40 driven simulation

Our ERA-40 driven simulation with an approximate downscaling factor of 2.5 is first performed as a control run for evaluating model performance. ERA-40 is observation based and thus contains less systematic biases compared to GCM outputs. Thus, the capability of CCLM to reproduce the present climate can be evaluated without, or at least with considerably reduced systematic bias in the large-scale forcing. The resolution difference between driving data and the CCLM can, however, lead to additional biases.

The first column of Figs. 2 and 3 shows the temperature and precipitation bias of the ERA-40 driven CCLM run compared to CRU and APHRODITE, respectively. The temperature bias ranges in most regions from  $-5$  to  $+5$  K with the exception of the Himalaya and especially the Karakorum where the bias ranges from  $-10$  to  $10$  K. Extreme biases ( $\pm 10$  K) are, however, only located at a few grid points and might result from an under-representation of the steep orography in the CCLM. The large observation uncertainty in this region can, however, also be a reason for the discrepancies (Brohan et al. 2006; Lorenz and Kunstmann 2012). The mountain ridges of the Tibetan Plateau and Indochina exhibit the strongest cold bias while the largest warm bias appears in the Tarim basin and western Mongolia. The cold bias in east Indonesia might be associated with the overestimation of precipitation, especially at the mountain ridges of New Guinea.

Figure 3 shows that the CCLM produces a pronounced relative wet bias in the most northern part of the domain (north of latitude  $40^\circ$ ) and over the Tibetan Plateau during their dry period (October to April, mainly in DJF and MAM). The high relative wet bias corresponds to a considerable absolute wet bias of up to 200 mm. However, the driving data ERA-40 has an even larger annual relative bias in this region (about 220 %) than the CCLM (Table 3), which can partially account for the CCLM's performance in this context. Similar results hold for east Indonesia and the Philippines, although the precipitation amounts in those regions are up to 10 times higher than over the Tibetan Plateau. The absolute wet bias in east Indonesia is about 1,500 mm. By contrast, the Philippines and west Indonesia show a surprisingly low bias compared to the spurious ERA-40 data in this region (Trenberth et al. 2001).

According to Table 3, CCLM does not significantly improve the area averaged bias for temperature compared to the driving data. This might be partially attributed to the rather small downscaling factor, which leads to similar orographic heights both in the forecast model used for ERA40 and in the CCLM. The overall warm bias of the ERA-40 driven CCLM run is 0.82 K, which is slightly higher than the bias of ERA-40. Concerning precipitation (see Table 3) the CCLM seems to be able to partly

compensate for the known spurious results of ERA-40 in the tropics (Trenberth et al. 2001) despite some significant relative biases in some subdomains. In summary, CCLM in this simulation setup is able to properly downscale the parent global fields and even reduces the error of the driving model ERA-40 within certain regions.

### 3.2 ECHAM5-20C driven simulation

As mentioned in Sect. 3.1, there will be a systematic bias compared to observations introduced by the driving GCM output into the CCLM. Further differences might be caused by the higher (compared to the ERA40-driven CCLM runs) downscaling factor of about 4.5 for the GCM driven CCLM runs, which can lead to different synoptic scale behaviour (Rummukainen 2010).

Two ECHAM5-driven CCLM runs are used to assess the influence of natural forcing. However, natural forcing affects only the driving GCM since the CCLM is not yet able to dynamically implement variable aerosol loads and a variable solar constant. Thus, natural forcing affects CCLM only implicitly via the driving model (mainly temperature).

The second and third columns of Fig. 2 show that both ECHAM5-20C driven runs basically produce the same bias patterns as the ERA-40 driven run. The differences between ERA-40 and ECHAM5-20C driven runs are small and restricted to south India, Indochina and the north east continental areas (NEC and NE). The ECHAM5-20C driven runs show a cold bias in every season in north-eastern China and other north-eastern subdomains, while in south India the most pronounced cold bias is mainly associated with the rainy season (JJA). Over Indochina, the ECHAM5-20C driven runs produce a slight warm bias in the annual mean temperature, in contrast to the cold bias of the ERA-40 driven run. There are no significant temperature pattern differences between ECHAM5-20C-R1 and ECHAM5-20C-all-R3. The biases averaged across the whole simulation domain for both runs differ only by about 0.2 K, which is of the same order of magnitude as the difference between the two driving datasets (shown in Tables 4, 5, where a total bias is 0.59 K for the ECHAM5-20C-R1 driven run and 0.41 K for the ECHAM5-20C-all-R3 driven run).

Concerning precipitation, both ECHAM5-20C driven runs produce similar bias patterns as the ERA-40 driven run (Fig. 3). Due to the seasonal precipitation cycle, the strongest absolute biases occur in MAM and JJA. The strong relative wet bias of CCLM from SON to MAM for all three driving datasets implies that the CCLM is not able to reproduce the dry season in the north sufficiently. In east Indonesia, the ECHAM5-20C driven runs produce a less pronounced wet bias in every season compared to the ERA-40 run, while in west Indonesia a more significant

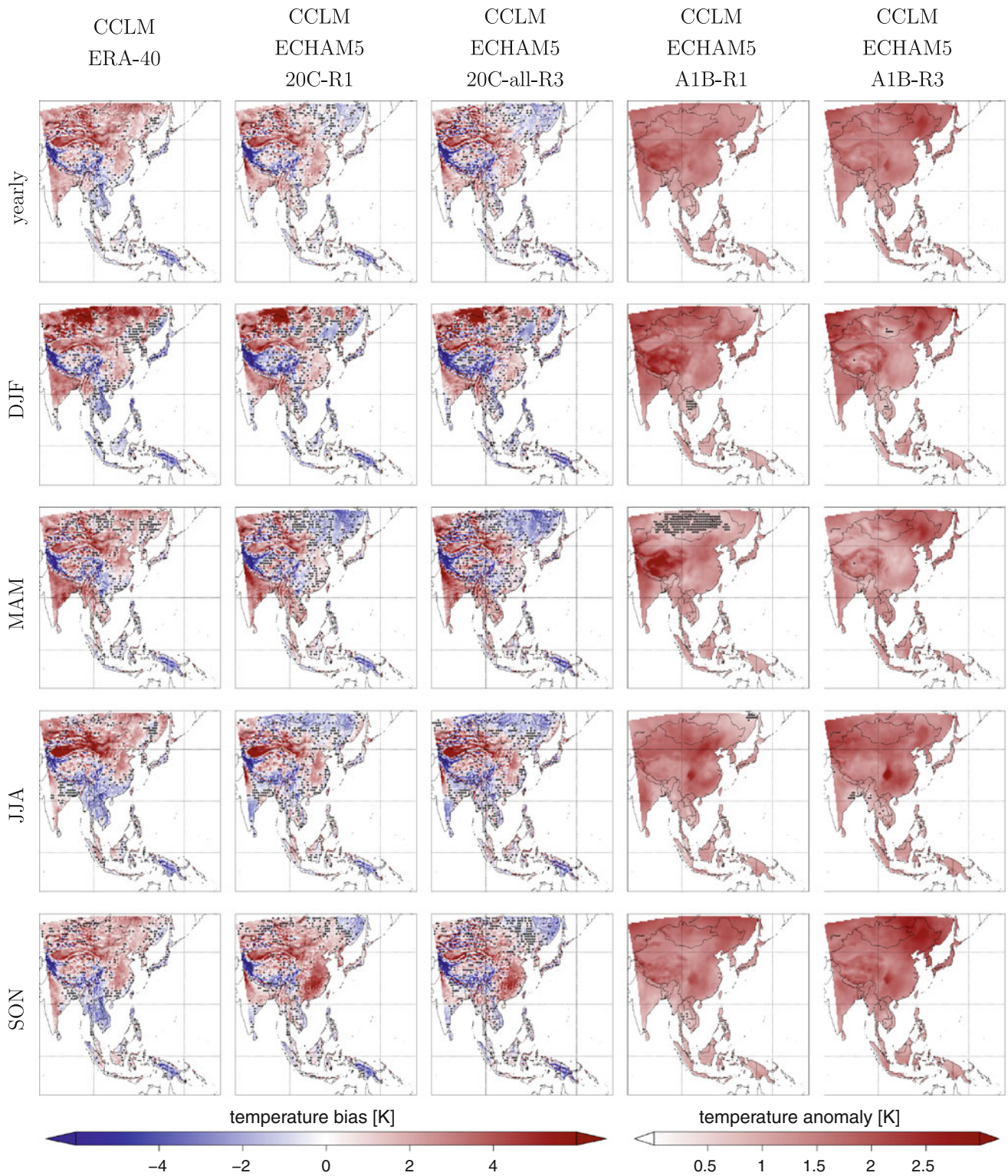


**Fig. 2** The temperature bias of the five simulations. The hindcast simulations over the period 1971–2000 are compared to CRU-TS3.0, while the future projections over the period 2021–2050 are compared

wet bias appears in the dry season (JJA) especially over the island of Java. Both ECHAM5-20C driven runs show again no significant difference. The overall precipitation biases

to their respective hindcast runs. *Shaded areas* indicate the regions with differences below 0.9 probability

across the CORDEX East Asia domain for ECHAM5-20C-R1 and ECHAM5-20C-all-R3 are 183 and 164 mm, respectively (Tables 4, 5).



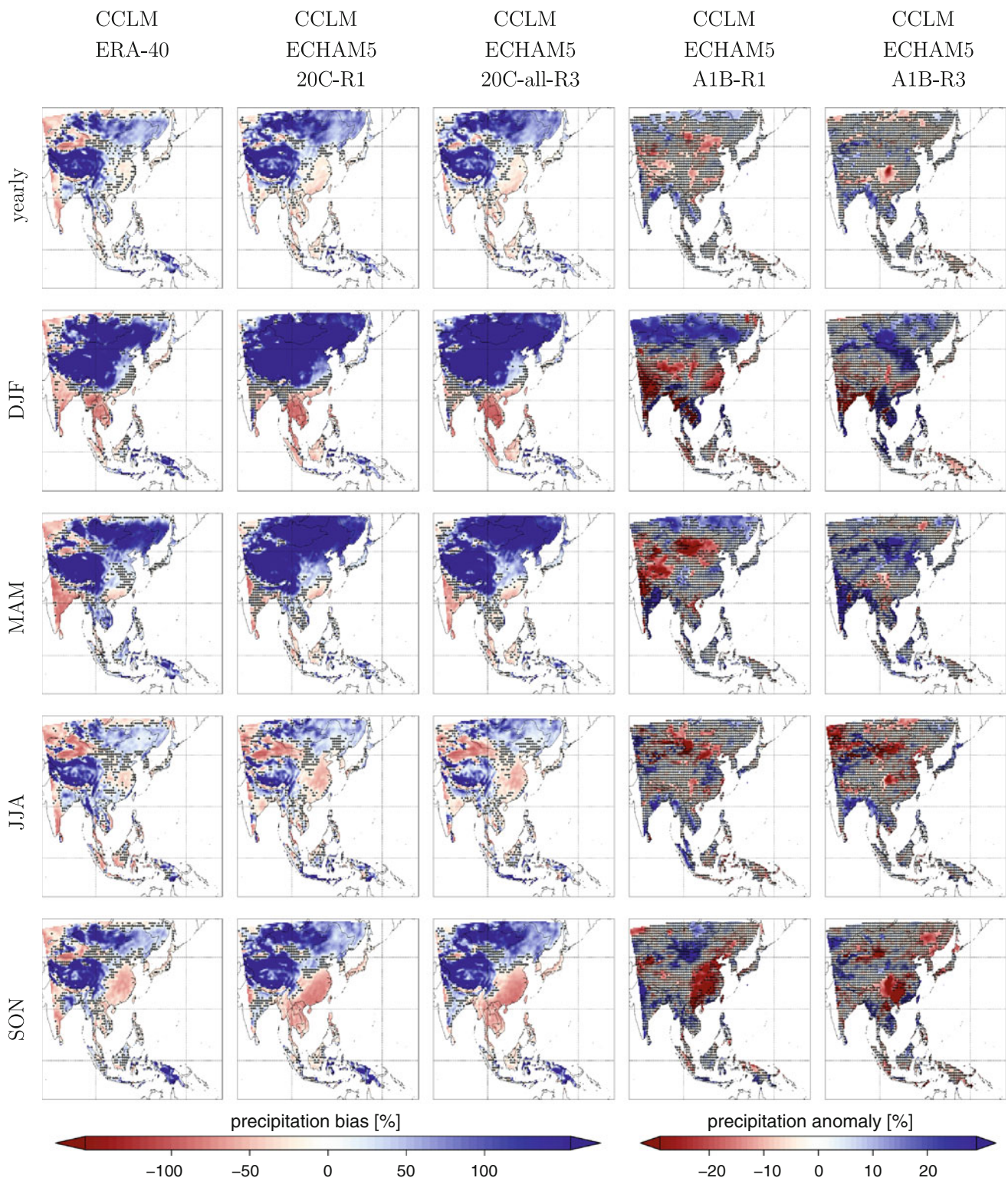


**Fig. 3** The relative precipitation bias of the five simulations. The hindcast simulations over the period 1971–2000 are compared to APHRODITE-APHRO\_V1003R1, while the future projections over

the period 2021–2050 are compared to their respective hindcast runs. *Shaded areas* indicate the regions with differences below 0.9 probability

Overall, there are no significant differences in the temperature and precipitation patterns for all three hindcast runs compared to the reference data. The CCLM produces

a small warm bias averaged over the whole CORDEX East Asia domain. The biases of the ECHAM5 driven runs are slightly lower than the ERA-40 driven run. The strongest

**Table 3** Annual mean 2 m temperature and averaged annual sum total precipitation bias for each subregion over the period 1971–2000. Shown here are the ERA-40 driven CCLM run and the respective ERA-40 biases compared to CRU-TS3.0 and APHRODITE for temperature and precipitation, respectively

Subregion	Temperature bias		Precipitation bias			
	CCLM	ERA-40	CCLM		ERA-40	
	[K]	[K]	[mm]	[%]	[mm]	[%]
Central China	0.39	−0.83	141.05	18.19	110.02	14.19
Central	−0.27	−0.49	478.82	31.42	348.99	22.90
East Indonesia	−0.88	0.11	1,530.18	88.55	3,454.35	199.89
Indo China	−0.69	0.01	325.64	22.82	653.68	45.80
North China	2.45	0.28	67.33	41.05	45.44	27.70
North East China	1.32	0.70	175.28	30.83	74.63	13.13
North East	0.73	1.48	217.05	30.21	217.53	30.28
North India	1.63	−1.32	291.15	28.44	65.66	6.41
North	2.28	1.30	139.02	44.40	290.48	92.78
North West	2.17	0.06	−39.67	−13.64	127.06	43.69
Philippines	−0.37	1.38	12.25	0.58	1,495.85	70.25
South China	0.29	0.34	−71.99	−5.18	−128.52	−9.24
South India	1.65	0.06	−227.12	−22.74	−95.90	−9.60
South Japan	−0.63	2.43	−231.80	−13.48	−224.97	−13.08
Tarim Basin	1.90	−1.34	103.97	113.06	235.40	255.98
Tibetan Plateau	−0.51	0.38	524.89	130.60	887.75	220.89
West Indonesia	0.01	−0.01	4.55	0.24	870.64	45.92
CORDEX-easia	0.82	0.22	239.86	28.02	471.53	55.08

biases generally occur at mountain ridges. CCLM simulates an average wet bias across the whole domain mainly due to an overestimation in the northern part of the simulation domain and over east Indonesia. The overestimation is more pronounced when driven by ECHAM5-20C. The hindcast driving data ECHAM5-20C-R1 and ECHAM5-20C-all-R3 show no significant differences over the whole domain, but ECHAM5-20C-all-R3 (with a natural forcing) leads to a lower bias for both temperature and precipitation compared to ECHAM5-20C-R1 (without a natural forcing) data. The same holds true for the respective CCLM simulations.

### 3.3 ECHAM5-A1B driven simulation

Two downscaled future projections based on Run-1 and -3 of ECHAM5 under the A1B emission scenario are performed for the period 2021–2050. Here, the CCLM model results are compared to the respective hindcast simulations driven by ECHAM5-20C-R1 and -all-R3, respectively.

The last two columns of Fig. 2 show the projected change of temperature. Both runs produce a similar annual temperature change with a slight south to north gradient of 1–2 K. The ECHAM5-A1B-R1 driven run has the most significant temperature increase over the Tibetan Plateau in DJF and MAM, while the ECHAM5-A1B-R3 driven run shows a stronger temperature increase in north-eastern

China throughout the year. Both runs reveal a more than 2 K temperature increase over the Sichuan Basin in JJA and SON. However, the ECHAM5-A1B-R3 driven run presents a more pronounced increase probably due to the effect of the natural forcing in the ECHAM5-20C-all-R3 driven run. The highest temperature increase of up to or above 3 K with the most extended spatial coverage is projected for winter from both runs, which is remarkable considering the time frame of only 30 years. The similar climate change signals were also detected in the previous studies of climate projections over east Asia (Xu et al. 2005; Zhang et al. 2012; Hulme et al. 1994) (Tables 6, 7).

Precipitation shows less systematic changes (Fig. 3) but large differences between both projections. The relative precipitation anomaly of the ECHAM5-A1B-R1 driven run displays an increase of precipitation in a band around 20°N and 50°N and a decrease elsewhere. The most significant decrease in absolute precipitation is projected for the North China Plain and central and southern China in autumn (SON). In JJA, precipitation is projected to increase by more than 15 % in west Indonesia, Indochina and south India. Nevertheless, due to the high variability of precipitation, these changes are not significant. This also explains the differences to the ECHAM5-A1B-R3 driven run and some findings of the previous studies (Xu et al. 2005; Zhang et al. 2012; Hulme et al. 1994), whose statements are, however, not based on the *t* test used in this paper. The



**Table 4** Annual mean 2 m temperature and averaged annual sum total precipitation bias for each subregion over the period 1971–2000

Subregion	Temperature bias		Precipitation bias			
	CCLM	ECHAM5-20C-R1	CCLM		ECHAM5-20C-R1	
	[K]	[K]	[mm]	[%]	[mm]	[%]
Central China	0.37	−2.34	92.62	11.95	692.65	89.34
Central	0.51	−0.37	282.23	18.52	−285.12	−18.71
East Indonesia	−0.68	1.81	1255.07	72.63	925.30	53.54
Indo China	0.53	−0.07	−265.16	−18.58	−127.29	−8.92
North China	1.69	0.50	124.86	76.12	121.00	73.77
North East China	0.13	−0.64	218.22	38.39	275.75	48.51
North East	−0.34	0.05	392.05	54.57	321.27	44.72
North India	1.93	−0.17	318.06	31.07	−144.08	−14.07
North	1.01	0.22	364.30	116.35	238.54	76.19
North West	2.06	1.23	123.10	42.33	7.64	2.63
Philippines	−0.33	2.04	−310.12	−14.57	852.57	40.04
South China	1.20	0.43	−297.92	−21.42	−129.42	−9.31
South India	0.54	−0.40	−104.06	−10.42	28.24	2.83
South Japan	0.10	4.22	−116.73	−6.79	−39.58	−2.30
Tarim Basin	1.71	−0.98	180.76	196.56	136.56	148.50
Tibetan Plateau	−1.01	1.03	472.09	117.46	683.47	170.06
West Indonesia	0.21	0.32	−246.59	−13.01	395.62	20.87
CORDEX-easia	0.59	0.28	183.48	21.43	221.59	25.88

Shown here are the ECHAM5-20C-R1 driven CCLM run and the respective ECHAM5-20C-R1 biases compared to CRU-TS3.0 and APH-RODITE for temperature and precipitation, respectively

ECHAM5-A1B-R3 driven run suggests that the projected significant temperature increase over the Sichuan Basin is related to a drastic precipitation decrease in the same region. The projections also hint at precipitation decreases of more than 20% over south China in autumn.

The temperature and precipitation change patterns derived from the CCLM results are comparable to the results from ECHAM5-A1B (figure not shown). Additionally, CCLM can reasonably simulate climate change signals on smaller scales, e.g. around the Tibetan Plateau for the ECHAM5-A1B-R1 driven run or over Sichuan Basin for the ECHAM5-A1B-R3 driven run.

### 3.4 Examples for resolved monsoon dynamics

Dynamical downscaling with RCMs is performed to better resolve dynamical processes using finer spatial and temporal scales. It is expected that the higher resolution leads to a more realistic representation of, e.g. convection and its influence on the regional climate than with the low resolution of the driving GCM. A dominant meso- $\alpha$  scale feature of east Asian meteorology is the East Asian Summer Monsoon (EASM), the representation of which by the CCLM we will exemplify in the following.

The quasi-stationary frontal system of the EASM is mostly disturbed by cyclonic vortices, which develop over the southwestern Tibetan Plateau and travel roughly along the Yangtze river (Wang 2006). These vortices are well known and even termed South-West Vortices (SWV). These disturbances are important ingredients to the generation of heavy rainfall events along the Meiyu band (Ding and Chan 2005). The SWVs are well resolved by the CCLM: an example is shown in Fig. 4, where the CCLM simulations are compared to the representation of such a situation by ECHAM5 (figure not shown). While the feature covers  $20 \times 20$  grid boxes in the CCLM simulations, the same area is represented in ECHAM5 by only  $4 \times 4$  grid boxes. Obviously, the coarse resolution of ECHAM5 cannot resolve such a vortex structure; thus, we expect that the CCLM better represents the humidity transport associated with the meso- $\alpha$  scale eddies and the intrinsic variability of the SWV. A more detailed analysis of the representation of such features in the CCLM and in ECHAM5 also in a statistical sense is beyond the scope of this paper and will be addressed in a follow-up study. This example gives, however, already an indication that the precipitation bias—also in the CCLM—might result at least in part from the parameterisation of precipitation

**Table 5** Annual mean 2 m temperature and averaged annual sum total precipitation bias for each subregion over the period 1971–2000

Subregion	Temperature bias		Precipitation bias			
	CCLM	ECHAM5-20C-all	CCLM		ECHAM5-20C-all-R3	
	[K]	[K]	[mm]	[%]	[mm]	[%]
Central China	0.46	−2.39	40.27	5.19	660.73	85.22
Central	0.29	−0.70	291.79	19.15	−243.62	−15.99
East Indonesia	−0.74	1.61	1172.01	67.82	935.84	54.15
Indo China	0.40	−0.26	−302.83	−21.22	−145.19	−10.17
North China	1.52	0.39	105.19	64.13	106.51	64.93
North East China	−0.19	−0.99	226.70	39.88	262.45	46.17
North East	−0.63	−0.48	403.50	56.16	312.59	43.51
North India	1.63	−0.33	263.97	25.79	−150.86	−14.74
North	0.75	0.00	388.45	124.07	249.66	79.74
North West	1.85	1.16	118.25	40.66	−4.16	−1.43
Philippines	−0.44	1.85	−356.47	−16.74	786.65	36.95
South China	1.05	0.13	−310.27	−22.31	−108.74	−7.82
South India	0.47	−0.52	−114.43	−11.46	6.39	0.64
South Japan	−0.05	3.94	−155.75	−9.05	−86.90	−5.05
Tarim Basin	1.62	−1.02	135.29	147.12	115.38	125.46
Tibetan Plateau	−1.16	0.97	464.60	115.60	671.69	167.13
West Indonesia	0.09	0.19	−310.80	−16.39	338.21	17.84
CORDEX-easia	0.41	0.09	164.58	19.23	212.46	24.82

Shown here are the ECHAM5-20C-all-R3 driven CCLM run and the respective ECHAM5-20C-all-R3 biases compared to CRU-TS3.0 and APHRODITE for temperature and precipitation, respectively

**Table 6** Annual mean 2 m temperature and total precipitation driven by ECHAM5-A1B-R1 over the period 2021–2050 compared to the hindcast run (1971–2000) driven by ECHAM5-20C-R1

Subregion	Temperature anomaly		Precipitation anomaly			
	CCLM	ECHAM5-A1B-R1	CCLM		ECHAM5-A1B-R1	
	[K]	[K]	[mm]	[%]	[mm]	[%]
Central China	1.57	1.43	−53.64	−6.18	2.55	0.17
Central	1.19	1.11	1.26	0.07	50.17	4.05
East Indonesia	0.98	1.04	−79.46	−2.66	−83.56	−3.15
Indo China	0.96	1.00	50.32	4.33	51.77	3.98
North China	1.48	1.68	−11.57	−4.01	−3.86	−1.35
North East China	1.41	1.46	8.03	1.02	2.94	0.35
North East	1.22	1.25	19.72	1.78	27.44	2.64
North India	1.49	1.56	19.35	1.44	4.60	0.52
North	1.44	1.61	25.43	3.75	33.78	6.12
North West	1.66	1.86	14.48	3.50	14.43	4.83
Philippines	0.97	0.98	109.59	6.02	107.69	3.61
South China	1.40	0.95	−45.66	−4.18	79.60	6.31
South India	1.25	1.36	62.20	6.95	27.55	2.68
South Japan	1.24	1.10	17.16	1.07	13.34	0.79
Tarim Basin	1.70	1.91	−21.29	−7.81	−17.25	−7.55
Tibetan Plateau	1.83	1.73	−32.59	−3.73	−22.01	−2.03
West Indonesia	1.01	1.02	13.46	0.82	92.93	4.06
CORDEX-easia	1.39	1.41	−2.02	−0.19	17.81	1.65

**Table 7** Annual mean 2 m temperature and total precipitation driven by ECHAM5-A1B-R3 over the period 2021–2050 compared to the hindcast run (1971–2000) driven by ECHAM5-20C-all-R3

Subregion	Temperature anomaly		Precipitation anomaly			
	CCLM	ECHAM5-A1B-R3	CCLM		ECHAM5-A1B-R3	
	[K]	[K]	[mm]	[%]	[mm]	[%]
Central China	1.48	1.37	−53.41	−6.55	1.28	0.09
Central	1.28	1.29	−18.72	−1.03	−3.75	−0.29
East Indonesia	1.12	1.17	−107.37	−3.70	−73.63	−2.76
Indo China	1.03	1.06	84.07	7.48	91.73	7.16
North China	1.55	1.68	0.88	0.33	16.41	6.07
North East China	1.78	1.84	−2.75	−0.35	34.99	4.21
North East	1.68	1.93	1.60	0.14	32.86	3.19
North India	1.40	1.30	38.52	2.99	68.44	7.84
North	1.69	1.84	−14.13	−2.01	−0.45	−0.08
North West	1.84	1.97	−4.63	−1.13	2.26	0.79
Philippines	1.08	1.10	111.32	6.28	64.24	2.20
South China	1.41	1.25	−33.72	−3.12	11.53	0.90
South India	1.26	1.37	55.99	6.33	17.72	1.76
South Japan	1.31	1.28	34.14	2.18	29.97	1.84
Tarim Basin	1.58	1.70	7.07	3.11	11.92	5.75
Tibetan Plateau	1.56	1.49	−6.83	−0.79	4.07	0.38
West Indonesia	1.13	1.14	36.00	2.27	119.65	5.36
CORDEX-easia	1.47	1.50	0.81	0.08	23.50	2.20

processes and/or the insufficient resolution of the tropopause height. East Asia is a region with strong fluctuation of the tropopause height. The bottom height of the upper Rayleigh sponge layer in CCLM is, however, held constant. Thus, the convection scheme might be unable to adequately represent the strong variability of tropical to sub-tropical monsoon processes. Furthermore, the moisture not condensed to precipitation in the south might be transported further north where it might lead to a positive precipitation bias.

To examine the internal EASM variability on the seasonal scale, the EASM index proposed by Wang and Fan (1999) and Wang et al. (2008) is applied to ECHAM5-20C-all-R3 and the CCLM run driven with the former. The resulting time series of both models is highly correlated ( $\rho = 0.90$ , significant at 1 % level) and shows that internal climate variability on the seasonal scale is transported well from the driving model to the driven model.

These results illustrate the capability of the CCLM both to represent small-scale monsoon features on the daily scale like SWVs and to maintain the internal variability on seasonal scale within the East Asia domain as provided by the driving GCM. A detailed analysis, based on post-processing the model outputs with a focus on dynamics to

receive a bias-corrected dataset, will be the focus of a forthcoming paper.

Similar dependence structures are expected for the East Asian Winter Monsoon (EAWM), i.e. a strong coherence of the dynamics between the driving model and the driven model and a better resolution of processes on higher frequencies by the CCLM. The first point could, however, not yet be tested as standard EAWM indices require dynamics north of 50 °C N (Jhun and Lee 2004; Li and Yang 2010), which coincides with the northern boundary of the simulation domain. The Siberian–Mongolian high (SMH) is a key component of the EAWM with high relevance due to its inter-annual variability (Wang 2006). Since the SMH is located close to the northern boundary of the CCLM domain, its fluctuations will be directly transported into the RCM. This assumption is supported by the example of a cold surge event shown in Figure 5 (still using the ECHAM5-20C-all-R3 driven simulation results), which is the main severe weather phenomenon during the EAWM season (Wang 2006). On January 4th, an extension of the SMH enters the CCLM domain. Consequently, a typical cold surge propagation of high pressure and associated cold air on ground level take place. It reaches its maximum on January 6th and weakens during an eastward drift afterwards.



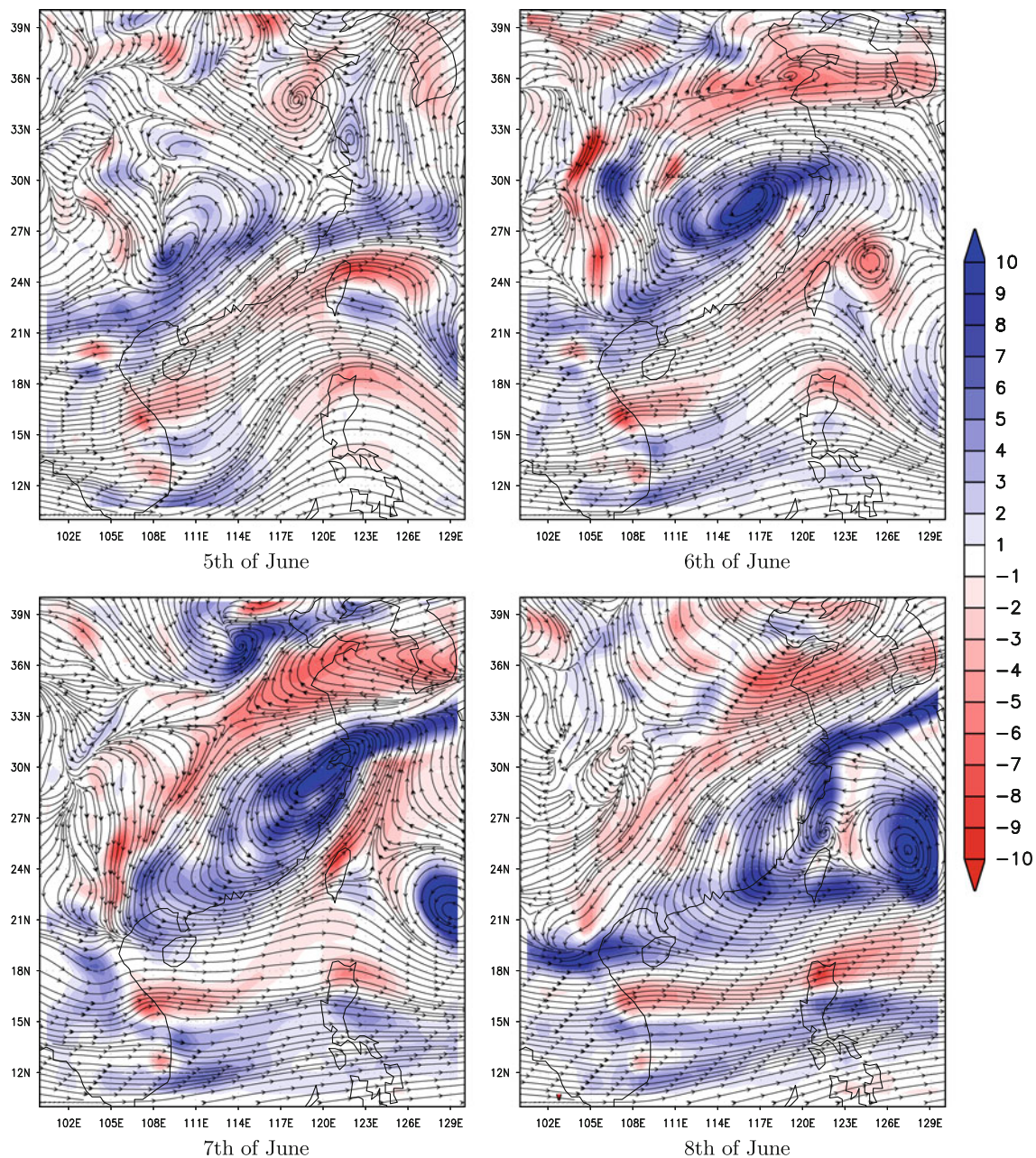


**Fig. 4** A case study of a Southwest Vortex, which occurred on the beginning of June over Southern China and is visible in the windfield at 850 hPa. The *arrows* at the streamlines show the wind direction.

The *shaded background* indicates the amplitude of the relative vorticity in  $10^{-5}/s$ . The data are taken from the CCLM run driven by ECHAM5-20C-all-R3

#### 4 Conclusions

The regional climate model COSMO-CLM (CCLM) is for the first time evaluated for its performance over East Asia following roughly the CORDEX recommendations. The paper analyses the annual and seasonal mean of temperature and precipitation by comparison with observations and between driving datasets and CCLM simulations. Examples are shown, which elucidate the merit of the higher spatial resolution for representing meso- $\alpha$ -scale processes

connected to monsoon dynamics. A more comprehensive analysis based on climate indices with focus on extreme climate events is on going and will be the focus of an upcoming publication.

The evaluation results demonstrate that the CCLM, with a proper parameter tuning for East Asia, can be used for downscaling parent global fields and partially improve the results of the driving model within certain regions. Overall the CCLM performs better in simulating 2 m temperature than precipitation. The significant cold bias over high



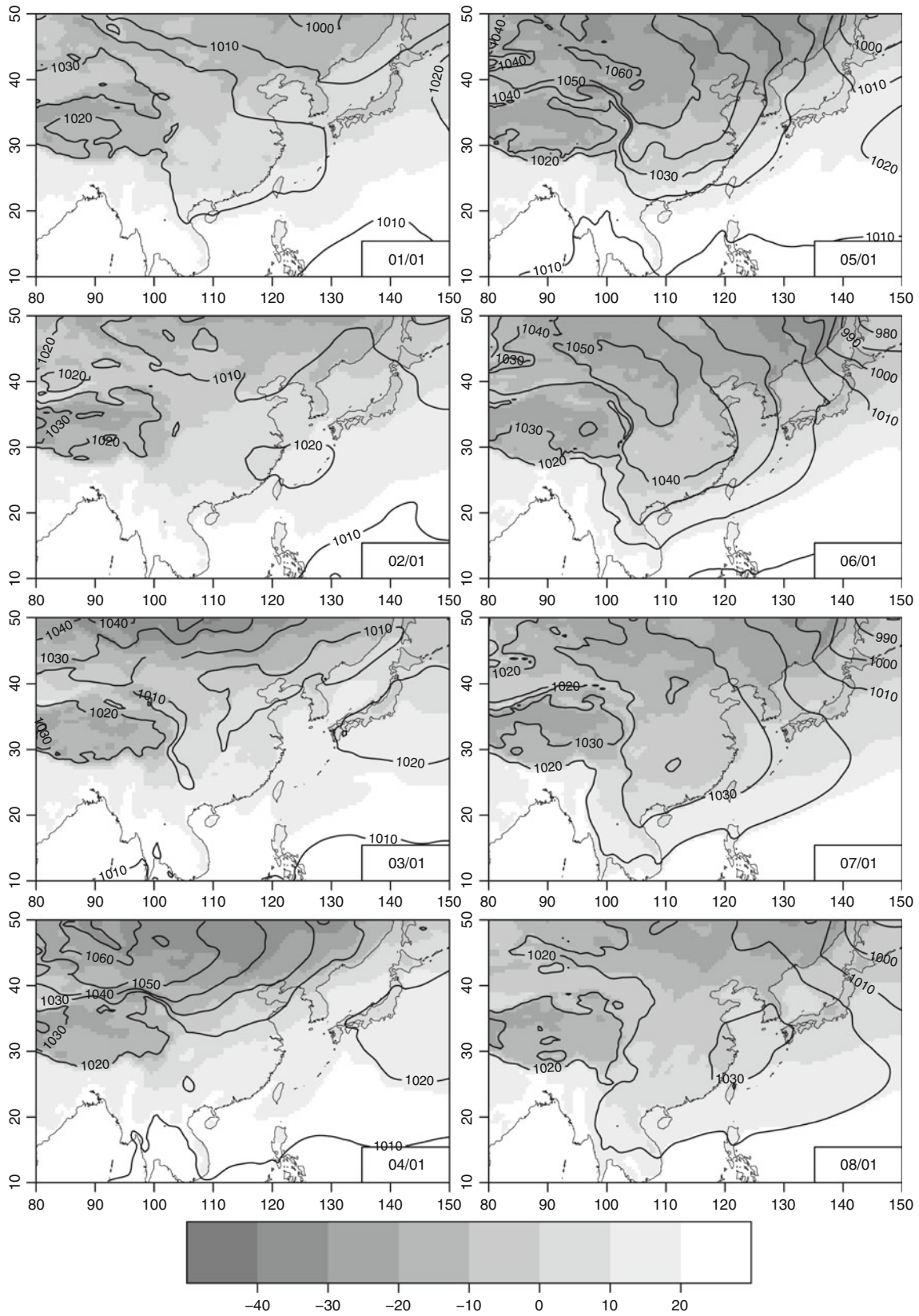


**Fig. 5** The analysis of sea level pressure and temperature at ground level shows a cold surge event. *Contour lines* mark isobars in hPa. The *shaded background* displays the 2 m temperature in °C

mountain ridges (Himalaya and New Guinea) seems to be related to a wet bias in the same regions. The CCLM produces a pronounced and spatially extended wet bias in the northern part of the domain and over the Tibetan Plateau in DJF and MAM. The differences between two ECHAM5-20C driven runs, one with and one without natural forcing in the forcing data, are not significant despite a somewhat lower bias of the former run.

Based on the positive evaluation results, the projected future climate change under the A1B scenario was investigated and suggests increases from 1 to 2 K in annual mean temperature across whole East Asia. The annual mean total precipitation, however, is not projected to change significantly. However, due to the much higher variability and the wider uncertainty range of precipitation compared to temperature, this conclusion is preliminary since only multi-ensemble-simulations can provide reliable estimates.

Finally, a few examples highlight the potential of the CCLM to reproduce and better resolve important East Asia monsoon dynamics: the internal variability of the driving GCM on the seasonal scales is well transferred into the CCLM domain and small-scale features of monsoon dynamics such as SWV and cold surge events which cannot be modelled by ECHAM5 are simulated by CCLM and provide added value to the downscaled results.

The simulation results will be available on the CERA data base at the World Data Centre for Climate in Hamburg for future applications and improvements.

**Acknowledgments** The work was funded by the DFG project (NDFG-SCHO-1384/1-1) and BMBF project (FK:02WM1042). ERA-40 reanalysis data was provided by ECMWF. Thanks also to the CLM-Community for providing the access to the model code and further guidance, especially to Dr. Burkhardt Rockel (Helmholtz-Zentrum Geesthacht Centre for Materials and Coastal Research).

## References

- Arakawa A, Lamb VR (1981) An energy and potential enstrophy conserving scheme for the shallow water equations. *Mon Weather Rev* 109(1):1836. doi:10.1175/1520-0493(1981)109<0018:APEAEC>2.0.CO;2
- Brohan P, Kennedy JJ, Harris I, Tett SFB, Jones PD (2006) Uncertainty estimates in regional and global observed temperature changes: a new data set from 1850. *J Geophys Res* 111(D12106). doi:10.1029/2005JD006548
- Ding YH, Chan JCL (2005) The east asian summer monsoon: an overview. *Meteorol Atmos Phys* 89(1–4):117–142. doi:10.1007/s00703-005-0125-z
- Dobler A, Ahrens B (2008) Precipitation by a regional climate model and bias correction in europe and south asia. *Meteorologische Zeitschrift* 17:499–509. doi:10.1127/0941-2948/2008/0306
- Fu CB, Wang SY, Xiong Z, Gutowski WJ, Lee DK, McGregor JL, Sato Y, Kato H, Kim JW, Suh MS (2005) Regional climate model intercomparison project for asia. *Bull Am Meteorol Soc* 86(2):257–266. doi:10.1175/BAMS-86-2-257
- Gao X, Xu Y, Zhao Z, Pal JS, Giorgi F (2006) On the role of resolution and topography in the simulation of east asia precipitation. *Theor Appl Climatol* 86(1–4):173–185. doi:10.1007/s00704-005-0214-4
- Giorgi F, Bates GT (1989) The climatological skill of a regional model over complex terrain. *Mon Weather Rev* 117(11):2325–2347(23). doi:10.1175/1520-0493(1989)117<2325:TCSOAR>2.0.CO;2
- Giorgi F, Jones C, Asrar G (2009) Addressing climate information needs at the regional level: the cordex framework. *WMO Bull* 58(3):175–183
- Hulme M, Zhao ZC, Jiang T (1994) Recent and future climate change in east asia. *Int J Climatol* 14(6):637–658. doi:10.1002/joc.3370140604
- IPCC (2007) Regional climate projections: the physical science basis in the fourth assessment report of the intergovernmental panel on climate change. IPCC.
- Jhun J, Lee E (2004) A new east asian winter monsoon index and associated characteristics of the winter monsoon. *J Clim* 17(4):711–726
- Ji YM, Vernekar AD (1997) Simulation of the asian summer monsoons of 1987 and 1988 with a regional model nested in a global gcm. *J Clim* 10(8):1965–1979. doi:10.1175/1520-0442(1997)010<1965:SOTASM>2.0.CO;2
- Jones P, Harris I (2008) Cru ts 3.1
- Kawase H, Yoshikane T, Hara M, Ailikun B, Kimura F, Yasunari T (2008) Downscaling of the climatic change in the mei-yu rainband in east asia by a pseudo climate simulation method. *SOLA* 4:73–76. doi:10.2151/sola.2008-019
- Kitoh A, Uchiyama T (2006) Changes in onset and withdrawal of the east asian summer rainy season by multi-model global warming experiments. *J Meteorol Soc Japan* 84(2):247–258. doi:10.2151/jmsj.84.247
- Kumar KR, Sahai AK, Kumar KK, Patwardhan SK, Mishra PK, Revadekar JV, Kamala K, Pant GB (2006) High-resolution climate change scenarios for india for the 21st century. *Curr Sci* 90(3):334–345
- Li Y, Yang S (2010) A dynamical index for the east asian winter monsoon. *J Clim* 23(15):4255–4262
- Lorenz C, Kunstmann H (2012) The hydrological cycle in three state-of-the-art reanalyses: Intercomparison and performance analysis. *J Hydrometeorol*. doi:10.1175/JHM-D-11-088.1
- Min SK, Park EH, Kwon WT (2004) Future projections of east asian climate change from multi-aogcm ensembles of ipccsres scenario simulations. *J Meteorol Soc Japan* 82(4):1187–1211. doi:10.2151/jmsj.2004.1187
- Rockel B, Geyer B (2008) The performance of the regional climate model clm in different climate regions, based on the example of precipitation. *Meteorologische Zeitschrift* 17:487–498. doi:10.1127/0941-2948/2008/0297
- Roeckner E (2005) IPCC MPI-ECHAM5\_T63L31 MPI-OM\_GR1.5L40 20C3M\_all run no.3: atmosphere 6 HOUR values MPImet/MaD Germany. World Data Center for Climate. CERA-DB, [http://cera-www.dkrz.de/WDCC/ui/Compact.jsp?acronym=EH5-T63L31\\_OM\\_20C3M\\_3\\_6H](http://cera-www.dkrz.de/WDCC/ui/Compact.jsp?acronym=EH5-T63L31_OM_20C3M_3_6H)
- Roeckner E, Lautenschlager M, Schneider H (2006a) IPCC-AR4 MPI-ECHAM5\_T63L31 MPI-OM\_GR1.5L40 20C3M run no.1: atmosphere 6 HOUR values MPImet/MaD Germany. World Data Center for Climate. [http://dx.doi.org/DOI:10.1594/WDCC/EH5-T63L31\\_OM-GR1.5L40\\_20C\\_1\\_6H](http://dx.doi.org/DOI:10.1594/WDCC/EH5-T63L31_OM-GR1.5L40_20C_1_6H)
- Roeckner E, Lautenschlager M, Schneider H (2006b) IPCC-AR4 MPI-ECHAM5\_T63L31 MPI-OM\_GR1.5L40 SRESA1B run no.1: atmosphere 6 HOUR values MPImet/MaD Germany. World Data Center for Climate. [http://dx.doi.org/DOI:10.1594/WDCC/EH5-T63L31\\_OM-GR1.5L40\\_A1B\\_1\\_6H](http://dx.doi.org/DOI:10.1594/WDCC/EH5-T63L31_OM-GR1.5L40_A1B_1_6H)



- Roeckner E, Lautenschlager M, Schneider H (2006c) IPCC-AR4 MPI-ECHAM5\_T63L31 MPI-OM\_GR1.5L40 SRESA1B run no.3: atmosphere 6 HOUR values MPImet/MaD Germany. World Data Center for Climate. [http://dx.doi.org/DOI:10.1594/WDCC/EH5-T63L31\\_OM-GR1.5L40\\_A1B\\_3\\_6H](http://dx.doi.org/DOI:10.1594/WDCC/EH5-T63L31_OM-GR1.5L40_A1B_3_6H).
- Rummukainen M (2010) State-of-the-art with regional climate models. *WIREs Clim Change* 1(1):82–96. doi:10.1002/wcc.008.
- Trenberth KE, Stepaniak DP, Hurrell JW, Fiorino M (2001) Quality of reanalyses in the tropics. *J Clim* 14(7):1499–1510. doi:10.1175/1520-0442(2001)014<1499:QORITT>2.0.CO;2.
- Uppala SM, Kllberg PW, Simmons AJ, Andrae U, Bechtold VDC, Fiorino M, Gibson JK, Haseler J, Hernandez A, Kelly GA, Li X, Onogi K, Saarinen S, Sokka N, Allan RP, Andersson E, Arpe K, Balmaseda MA, Beljaars ACM, Berg LVD, Bidlot J, Bormann N, Caires S, Chevallier F, Dethof A, Dragosavac M, Fisher M, Fuentes M, Hagemann S, Hlm E, Hoskins BJ, Isaksen L, Janssen PAEM, Jenne R, McNally AP, Mahfouf JF, Morcrette JJ, Rayner NA, Saunders RW, Simon P, Sterl A, Trenberth KE, Untch A, Vasiljevic D, Viterbo P, Woollen J (2005) The era-40 reanalysis. *Q J R Meteorol Soc* 131(612):2961–3012. doi:10.1256/qj.04.176, URL:<http://dx.doi.org/10.1256/qj.04.176>.
- von Storch H, Zwiers F (1999) *Statistical analysis in climate research*. Cambridge University Press, Cambridge
- Wang B (2006) *The Asian monsoon*. Springer, Berlin
- Wang B, Fan Z (1999) Choice of south asian summer monsoon indices. *Bull Am Meteorol Soc* 80:629–638
- Wang B, Wu Z, Li J, Liu J, Chang C, Ding Y, Wu G (2008) How to measure the strength of the east asian summer monsoon. *J Clim* 21(17):4449–4463
- Williams PD (2009) A proposed modification to the robert–asselin time filter. *Mon Weather Rev* 137(8):2538–2546. doi:10.1175/2009MWR2724.1
- Xie P, Yatagai A, Chen M, Hayasaka T, Fukushima Y, Liu C, Yang S (2007) A gauge-based analysis of daily precipitation over east asia. *J Hydrometeorol* 8(3):607–626. doi:10.1175/JHM583.1
- Xu Y, Zhao Z, Luo Y, Gao X (2005) Climate change projections for the 21st century by the ncc/iap t63 with sres scenarios. *Acta Meteorol Sin* 19:407–417
- Yatagai A, Arakawa O, Kamiguchi K, Kawamoto H, Nodzu MI, Hamada A (2009) A 44-year daily gridded precipitation dataset for asia based on a dense network of rain gauges. *Sci Online Lett Atmos (SOLA)* 5:137–140. doi:10.2151/sola.2009-035
- Yhang YB, Hong SY (2008) Improved physical processes in a regional climate model and their impact on the simulated summer monsoon circulations over east asia. *J Clim* 21(5):963–979. doi:10.1175/2007JCLI1694.1
- Zhang L, Wu T, Xin X, Dong M, Wang Z (2012) Projections of annual mean air temperature and precipitation over the globe and in china during the 21st century by the bcc climate system model bccsm1. *Acta Meteorol Sin* 26(3):362–375. doi:10.1007/s13351-012-0308-8